



HAL
open science

Combined effect of Pt and W alloying elements on Ni-silicide formation

T. Luo, Dominique Mangelinck, M. Descoins, M. Bertoglio, N. Mouaici, A.
Hallén, Christophe Girardeaux

► **To cite this version:**

T. Luo, Dominique Mangelinck, M. Descoins, M. Bertoglio, N. Mouaici, et al.. Combined effect of Pt and W alloying elements on Ni-silicide formation. *Journal of Applied Physics*, 2018, 123 (12), pp.125301. 10.1063/1.5020435 . hal-02044799

HAL Id: hal-02044799

<https://amu.hal.science/hal-02044799>

Submitted on 14 Feb 2022

HAL is a multi-disciplinary open access archive for the deposit and dissemination of scientific research documents, whether they are published or not. The documents may come from teaching and research institutions in France or abroad, or from public or private research centers.

L'archive ouverte pluridisciplinaire **HAL**, est destinée au dépôt et à la diffusion de documents scientifiques de niveau recherche, publiés ou non, émanant des établissements d'enseignement et de recherche français ou étrangers, des laboratoires publics ou privés.

Combined effect of Pt and W alloying elements on Ni-silicide formation

T. Luo^{a,*}, D. Mangelinck^b, M. Descoins^a, M. Bertoglio^b, N. Mouaici^c, A. Hallén^d, C. Girardeaux^a

^a Aix-Marseille Université, CNRS, IM2NP, Faculté Saint Jérôme, Case 142, 13397 Marseille Cedex 20, France

^b CNRS, Aix-Marseille Université, IM2NP, Faculté Saint Jérôme, Case 142, 13397 Marseille Cedex 20, France

^c Ecole Nationale des Mines et de la Métallurgie ENSMM-Annaba, Ex CEFOS Chaiba BP 233 RP Annaba, W129, Sidi Amar, Algeria

^d KTH Royal Institute of Technology, School of Information and Communication Technology (ICT), SE-164 40 Kista-Stockholm, Sweden

Abstract: A combinatorial study of the combined effect of Pt and W on Ni silicides formation is performed. Ni(Pt, W) films with thickness and composition gradients were prepared by a co-deposition composition spread technique using sputtering deposition from Pt, W and Ni targets. The deposited Ni(Pt,W) films were characterized by X-ray diffraction, X-ray reflectivity, Rutherford backscattering and atom probe tomography. The maximum content of alloying elements is close to 27 at.%. Simulations of the thickness and composition were carried out and compared with experimental results. *In-situ* X-ray diffraction and atom probe tomography were used to study the phase formation. Both additive alloying elements (Pt+W) slow down the Ni consumption and the effect of W is more pronounced than the one of Pt. Regarding the effect of alloying elements on Ni silicides formation, three regions could be distinguished in the Ni(Pt,W)/Si wafer. For the region close to the Ni target, the low contents of alloying elements (Pt+W) have

* Corresponding author, e-mail: ting.luo@im2np.fr

little impact on the phase sequence (δ -Ni₂Si is the first silicide and NiSi forms when Ni is entirely consumed) but the kinetics of silicide formation slows down. The region close to the Pt target has high contents of (Pt+W) and is rich in Pt and a simultaneous phase formation of δ -Ni₂Si and NiSi is observed. For the high (Pt+W) contents and W-rich region, NiSi forms unexpectedly before δ -Ni₂Si and the subsequent growth of δ -Ni₂Si is accompanied by the NiSi consumption. When Ni is entirely consumed, NiSi regrows at the expense of δ -Ni₂Si.

Keyword: Ni silicides; Pt and W additive; Co-sputtering; Reactive diffusion

1. Introduction

With the downscaling of microelectronic devices, NiSi has been widely used as contacts in complementary-metal-oxide-semiconductor (CMOS) transistors for source, drain and gate.¹⁻⁴ Compared to the former contact materials of CoSi₂ and TiSi₂, NiSi has attractive advantages including low resistivity, less Si consumption and Ni diffusion controlled reaction.⁵ However, it also confronts with several challenges which can be deduced from the Ni-Si phase diagram. Indeed, in the Ni-rich region of the phase diagram, there are five metal-rich phases, resulting in a complex phase sequence and a high risk of early roughness of interfaces. In the Si-rich region of the phase diagram, the presence of the NiSi₂ phase with a high resistivity indicates that NiSi is not stable on the Si substrate and may transform to NiSi₂, which usually nucleates at 700°C~800°C. Agglomeration is another degradation mechanism of NiSi at intermediate temperature (500°C~700°C). This leads to a degradation of the contact resistance. The phase stability (phase transformation from NiSi to NiSi₂) and morphological stability of NiSi (agglomeration) are influenced by many factors, including the initial thickness of Ni, the type of the Si substrate, the NiSi texture.⁶

It has been shown that additive alloying elements could substantially increase the phase stability and the morphological stability of nickel monosilicide.^{5,7-9} Mangelinck *et al.*^{7,9} have shown that the addition of 5 at. % Pt in the Ni film can increase the temperature of NiSi₂ nucleation and delay the agglomeration of NiSi by more than 100°C. Lavoie *et al.*⁵ have shown that additions of Pt, Pd and Rh are most efficient to delay the formation of NiSi₂ while elements such as W, Mo, Re, and Ta are amongst the most efficient elements to delay the NiSi agglomeration. Moreover, both Pt¹⁰ and W⁸ have an impact on the texture of NiSi by inducing epitaxial orientations and limiting axiotaxy, leading to a better morphological stability of NiSi. Therefore, it might be interesting to combine the positive effect of Pt and W on the stability of NiSi in order to obtain an optimized system.

However, adding alloying element of Pt or W to Ni film could significantly modify the sequence of Ni silicides formation at low temperature (metal-rich phases). For Ni(3 at.% Pt), the sequential phase formation of δ -Ni₂Si and NiSi has been observed.¹¹ With increasing the content of Pt to 10 to 13 at.%, θ -Ni₂Si appears as the first silicide. For *in-situ* XRD measurement, the growth of θ -Ni₂Si is characterized by the absence of XRD peaks during the consumption of the metal due to the epitaxial relationship on the Si substrate.¹²⁻¹⁴ In comparison to the well-studied Ni(Pt)-Si system, the effect of W on phase sequence is less understood. For Ni(10 at.% W), Derafa *et al.*¹⁵ found that Ni₃₁Si₁₂ probably forms during the deposition of Ni film and that another unknown silicide Ni_xSi_y appears at the end of the Ni consumption. However, Deduytsche *et al.*⁸ found that the phase sequence for Ni(10 at.% W) is similar to that of Ni(10 at.% Pt), with no metal-rich phases detected by XRD suggesting the formation of θ -Ni₂Si before the appearance of NiSi.¹³

The purpose of this work is to investigate the combined effect of Pt and W on the Ni silicides formation by combinatorial analysis. Indeed, combinatorial analysis is a fast and efficient method to investigate a system. Many methods for high-throughput synthesis have been developed¹⁶ and

the co-deposited composition spread (CCS) technique has proven to be an especially versatile method for forming a wide range of compositions in a single experiment. In this method, thin films are deposited by physical vapor deposition on a substrate simultaneously, from two or more sources that are spatially separated and chemically distinct, producing a film with an inherent composition gradient and intimate mixing of the constituents. In this work, the co-deposited composition spread technique was used to produce Ni films alloyed with both Pt and W that present gradient in composition and thickness. As-deposited samples were characterized by several experimental methods and simulation of the corresponding co-deposition was carried out for comparison. The silicide formation and the redistribution of the elements were monitored by *in-situ* X-ray diffraction (XRD) and atom probe tomography (APT). The formation sequence of Ni silicides is examined as a function of the contents of alloying elements which are related to the position on the wafer. The combined effect of Pt and W is discussed accordingly.

2. Experiment

Ni films with alloying elements of Pt and W were deposited on Si(100) at room temperature. Three targets of Ni, Pt and W were used together in a coaxial magnetron sputtering system to deposit films with thickness and composition gradients on stationary substrates [Fig. 1(a)]. The Si substrate was immersed into a 5% dilute HF solution for 1 min to remove the native oxide prior loading into the sputtering chamber. The deposition was performed with a base pressure of $\sim 10^{-8}$ Torr using 99.9999% pure Ar gas flow. The deposition rate as a function of applied power was calibrated for each target. During the co-sputtering, the following powers were applied respectively on Ni, Pt and W targets: 181W (DC), 18W (DC) and 43W (RF), and the corresponding deposition rates are 0.6, 0.1 and 0.05 nm/s. The deposition time was chosen in order to have thickness in the range 30-70nm, since the phase sequence should not depend too much on the film thickness for

this thickness range. Indeed, the phase sequence is expected to be very different for thickness smaller than 10nm or larger than 100nm.

After deposition, the wafer was divided into 42 pieces (approximately 10mm×19mm) according to the pattern shown in Fig. 1(b). In the following, we will refer to this numbering: for instance, Sample 1 in the wafer will be named “S1”. All the as-deposited samples were characterized by X-ray diffraction (XRD) and X-ray reflectivity (XRR) while atom probe tomography (APT) and Rutherford backscattering spectrometry (RBS) were carried on selected samples. XRD and XRR were performed using the Bragg–Brentano geometry with a Cu K α source and a rapid detector (PANalytical X’Celerator). RBS was performed with a 2 MeV He⁺ and a 165° beam backscattering angle. Samples were tilted 7 degrees to avoid channeling. The RUMP program¹⁷ was used to fit the results of RBS.

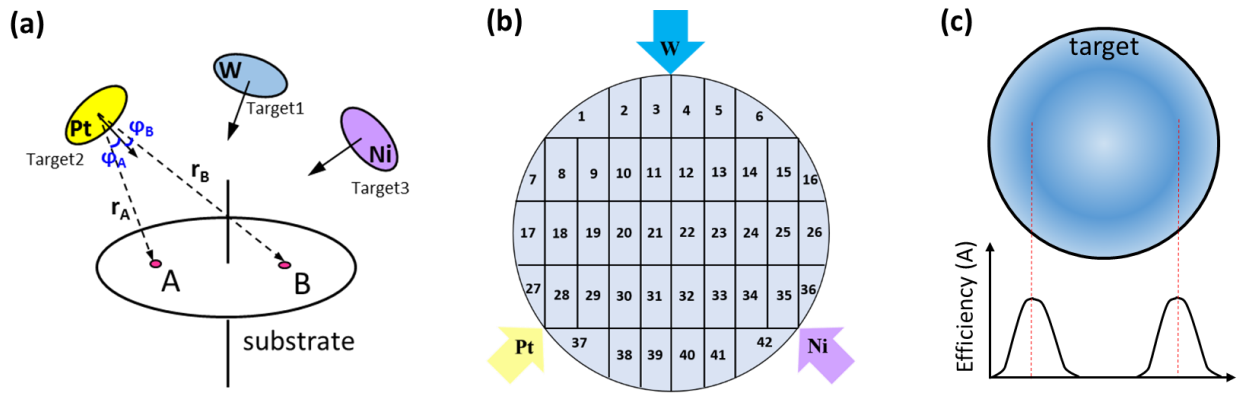


Fig. 1. Schematic diagrams of (a) the magnetron sputtering with three targets of Ni, Pt and W; (b) the sample cutting pattern; (c) the evaporation efficiency along the diameter of a target.

In-situ XRD measurements were performed on half of the 42 samples from 150°C to 400°C under a vacuum of $\sim 10^{-5}$ mbar. The temperature was firstly increased from room temperature to 150 °C at a rate of 35 °C/min. Then from 150 °C to 400°C, the temperature was increased by steps of 5°C and a 4 min-XRD scan was performed at a constant temperature after each step. The heating

rate between two steps was 10 °C/min. The same *in-situ* XRD measurements were done but stopped at two other annealing temperatures (295°C and 345°C) to study specific stages of the silicides formation and APT measurements were also carried on these two annealed samples.

Needle-shaped specimens were prepared for APT measurements by focused ion beam (FIB) equipped with a micromanipulator and the detailed steps have been described elsewhere¹⁸. The APT analyses were carried out in a LEAP 3000X HR instrument. The laser pulsing rate was kept at 100 kHz and the detection rate at 0.002 event/pulse by increasing the applied voltage. The specimen temperature was 50 K and the laser energy was set between 0.9 nJ and 1.4 nJ. Data reconstruction was done with the commercial IVAS software.

3. Results

3.1. As-deposited samples

3.1.1 Experimental results from XRR, XRD, APT and RBS.

As deposited Ni(Pt,W) film on Si wafer was divided into 42 pieces according to the pattern shown in Fig. 1(b). Determined from the fringe period in XRR spectra, the thickness of Ni(Pt,W) film varies from 22 to 67nm.

XRD was used to roughly characterize the Ni(Pt,W) film composition based on the shift of Ni diffraction peak. Compared to the standard XRD spectrum of pure Ni, a shift in the diffraction angle (2θ) toward **small angles** could be observed for Ni(Pt, W) film and it changes with the layer composition. This diffraction peak shift may be due to the strain effect or due to the increase in the lattice parameter of thin Ni(Pt,W) film. It has been found that the peak shift for pure Ni film is small¹⁹, indicating a weak strain effect in the thin Ni film. Although the additive alloying elements of Pt and W may introduce extra strain to the Ni(Pt,W) layer, this effect is assumed to be small.

Additive Pt and W should thus account for the XRD peak shift by increasing the inter-planar distance d_{hkl} , which could be calculated by Bragg's law. On the basis of d_{hkl} , the lattice parameter of $a_{Ni(Pt,W)}$ could then be determined by assuming a fcc structure of Ni(Pt,W) film. The concentration of alloying elements could be estimated from the Vegard's law by using the lattice parameter of Ni, Pt and W at room temperature:

$$a_{Ni(Pt,W)} = (1-x-y) a_{Ni} + xa_{Pt} + ya_{W} \quad (1)$$

Here $a_{Ni} = 3.535 \text{ \AA}$ and $a_{Pt} = 3.924 \text{ \AA}$, a_w is unknown because of the bcc structure of W and was assumed to be equal to a_{Pt} . x and y represent the atomic concentration of Pt and W respectively. It is impossible to determine the individual concentration of Pt and W only from the XRD peak shift but the total alloying elements concentration can be estimated. However, this calculation is not very accurate because the assumed a_w , and the possible weak strain effect of alloying elements on the thin film would contribute uncertainties to the calculated compositions. Nevertheless, this calculation based on the XRD peak shift is still an easy and effective method to estimate the total contents of alloying elements, which vary from 6 to 42 at.%. More accurate thickness and composition of three specific samples (S08, S28 and S34) were obtained by APT or RBS and the results are shown in Table 1.

Table 1. Thickness and composition of Ni(Pt,W) film characterized by XRR, XRD, APT and RBS, with the corresponding simulation results (Sim).

	S08			S28			S34		
	XRR/ XRD	APT	Sim	XRR/ XRD	RBS	Sim	XRR/ XRD	RBS	Sim
h (nm)	31	30	31	33	33	37	59	55	65
Pt (at. %)	--	20	15	--	20	22	--	5	6
W (at. %)	--	7	9	--	5	5	--	3	3
(Pt+W) at. %	36	27	24	38	25	27	10	8	9

3.1.2 Simulation results

Simulations of the thickness and composition of Ni(Pt,W) film were carried out by considering the lateral distributions of particle (vapor) fluxes. Following the work of Rother *et al.*²⁰, the distribution of particle fluxes for point-like sources can be expressed as the following equation:

$$j = \frac{A}{r^2} (\cos\varphi)^n \quad (2)$$

Here, j is the vapor particle flux, A is used to characterize the absolute value of the flux, r is the distance between the source and the substrate, φ is the angle between the source normal and the considered direction [shown in Fig. 1(a)], n is the lateral vapor distribution coefficient, which was estimated as 2.²¹

In order to simulate the co-sputtering of Pt, W and Ni, each target is treated as a round-plate source and is divided into smaller regions that are considered as point-like sources. For a given point in the substrate, the parameters of r and φ vary with the position of these point-like sources. Furthermore, A is not considered as a constant value, but changes with the radial position in the

source. Indeed, the target surface is not flat after the magnetron sputtering and a circular deeper erosion zone could be observed at half radius position in the target. It indicates a variable sputtering efficiency within the target because of the magnetron effect. The Gaussian distribution was used to fit the real profile of the sputtering efficiency as a function of the radial position in the target [Fig. 1(c)].

Figure 2 shows the simulation results of the thickness and composition gradients of Ni(Pt,W) film. With increasing the distance between one target and the substrate, the corresponding element concentration varies relatively in an elliptical profile. The contents of alloying elements are in the range of 4 to 23 at.% for Pt and 2 to 14 at.% for W. The film thickness changes from 30 to 65 nm.

In order to evaluate the result of simulation, a comparison has been made between experimental and simulation results. The average difference in thickness characterized by XRR and simulation is 4.6 nm, which is quite acceptable considering the maximum thickness of 65 nm. Meanwhile, the average difference between XRD and simulation on the contents of alloying elements is 4.9 at.%. Even though this value is slightly high, one should be aware of that the contents of alloying elements deduced from XRD peak shift is not very accurate (see 3.1.1). For three specific samples of S08, S28 and S34, the thickness and composition characterized by experimental techniques (XRR, XRD, APT or RBS) have been compared with simulation results (Table 1). The differences between XRD-based compositions and simulation results increase with the contents of alloying elements, but the results of XRR, APT, RBS are in good accordance with simulation results. Therefore, simulation results of the thickness and composition of Ni(Pt,W) film are reliable and the deposition method allows to design a Ni film with composition gradients of Pt and W on the same wafer. In the following, the concentrations used to interpret the silicide formation would be the ones obtained by simulation.

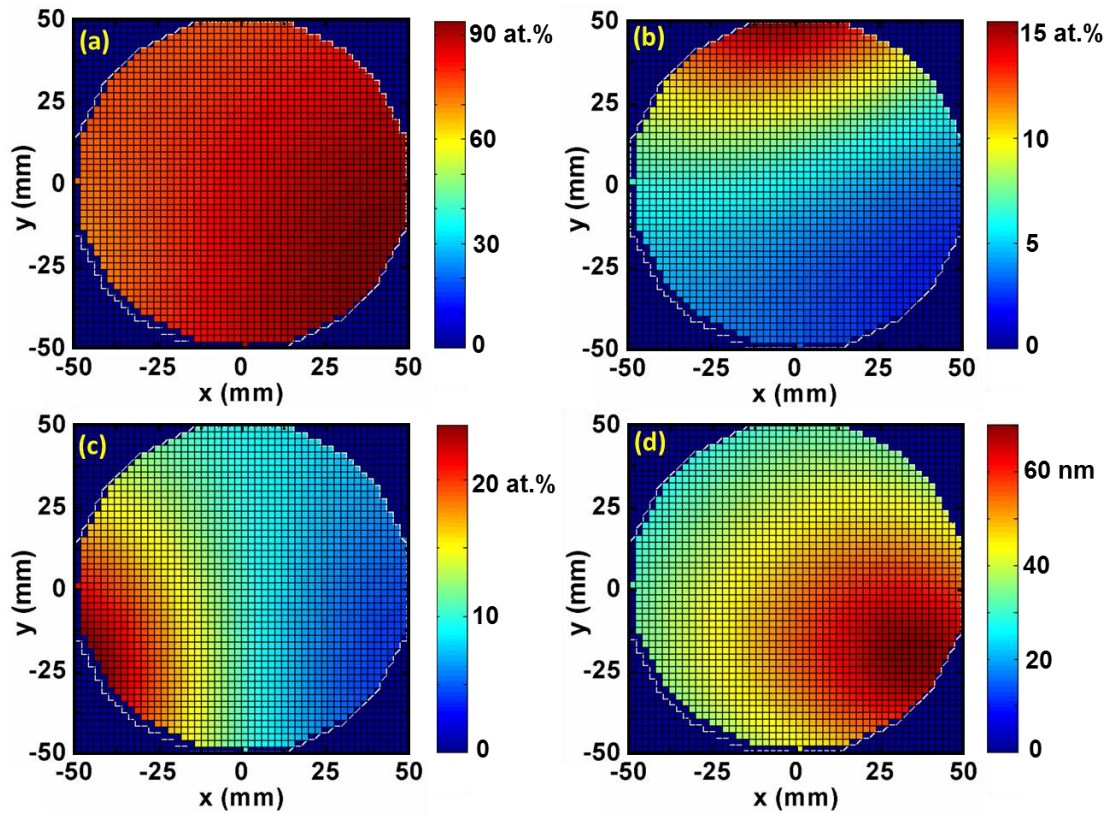


Fig. 2. Simulation results of the atomic content of (a) Ni, (b) Pt, (c) W, and of (d) thickness (nm).

3.2 Ni-silicide formation

In-situ XRD measurements were performed from 150°C to 400°C on half of the 42 samples (odd number samples) to study the formation sequence of Ni silicides. Regarding the combined effect of Pt and W on Ni silicides formation, three composition regions are distinguished in the Ni(Pt,W)/Si wafer (Fig. 2): low (Pt+W)% region, high (Pt+W)% and Pt-rich region, and high (Pt+W)% and W-rich region. Typical *in-situ* XRD results of three composition regions are shown in Fig. 3

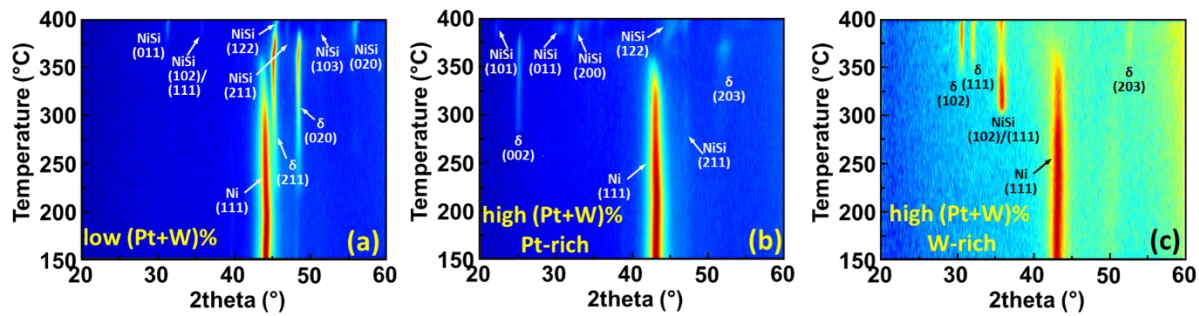


Fig. 3. Typical *in-situ* XRD results for: (a) low (Pt+W)% region (b) high (Pt+W)% and Pt-rich region; and (c) high (Pt+W)% and W-rich region

The region of Ni(Pt,W)/Si wafer close to the Ni target is characterized with large film thickness and low contents of alloying elements. One representative *in-situ* XRD result (S35) is shown in [Fig. 3(a)]. The simulated thickness and composition for S35 are 67 nm and 7.2 at.% (4.7 at.% Pt and 2.5 at.% W). A simple phase sequence is observed. Only one Ni(111) peak could be detected at around 44° from 150°C, until two peaks of δ -Ni₂Si (45.3° and 48.5°) appear at 215°C. δ -Ni₂Si exists over a large temperature range from 215°C to 400°C and the total consumption temperature of Ni has been delayed to 375°C. Afterwards, NiSi appears with six different peaks and grows by consuming δ -Ni₂Si. At the end of the annealing, NiSi is the unique silicide present in the film.

For the region of Ni(Pt,W)/Si wafer close to the Pt target, the contents of alloying elements are relative high and the major alloy is Pt. The alloying elements contents of one typical sample S29 are 19 at.% Pt and 4 at.% W. The *in-situ* XRD measurement of S29 [Fig. 3(b)] shows a different phase sequence from the former region with low (Pt+W) contents. The peak of the metal phase (~44°) decreases in intensity, indicating the growth of another phase (certainly θ -Ni₂Si). However, the peak is present until one peak of δ -Ni₂Si (25.3°) and another peak of NiSi (47.3°) are detected simultaneously at 280°C. During the subsequent growth of δ -Ni₂Si by the consumption of Ni,

another peak of δ -Ni₂Si appears at $\sim 52^\circ$. Ni is completely consumed around 370°C. Afterwards, NiSi grows clearly at the expense of δ -Ni₂Si and becomes the unique phase at 400°C.

The region of Ni(Pt,W)/Si wafer close to the W target contains a large amount of alloying elements with a majority of W. From the simulation of S03, the contents of Pt and W are 9.8 at.% and 14 at.%, respectively. An unusual phase sequence has been observed in this region and one typical result of S03 is shown in Fig. 3(c). Only the metal peak is present until 305°C, at which temperature another peak corresponding to NiSi appears at 36.1° . With increasing the temperature to 345°C, two peaks of δ -Ni₂Si surprisingly appear at 30.6° and 32.3° . *In-situ* XRD result does not provide any evidence for the formation of metal rich phases before the appearance of NiSi. The increase of the δ -Ni₂Si peak intensity is accompanied by the decrease of the NiSi peak intensity. When the metal layer is entirely consumed, the NiSi peak intensity increases again by consuming δ -Ni₂Si. At the end of the *in-situ* XRD measurement, both δ -Ni₂Si and NiSi exist.

4. Discussion

4.1 Metal consumption and first phase formation

In order to compare the kinetics of metal consumption for the three different regions, normalized intensities of the metal peak are shown as a function of temperature in Fig. 4. Additive alloying elements of Pt and W could actually slow down the speed of the metal consumption, rendering a higher total consumption temperature compared to the case of pure Ni.²² This is in accordance with the former investigation by Lavoie *et al.*⁵. Moreover, W is more efficient to decrease the consumption rate of Ni compared with Pt.

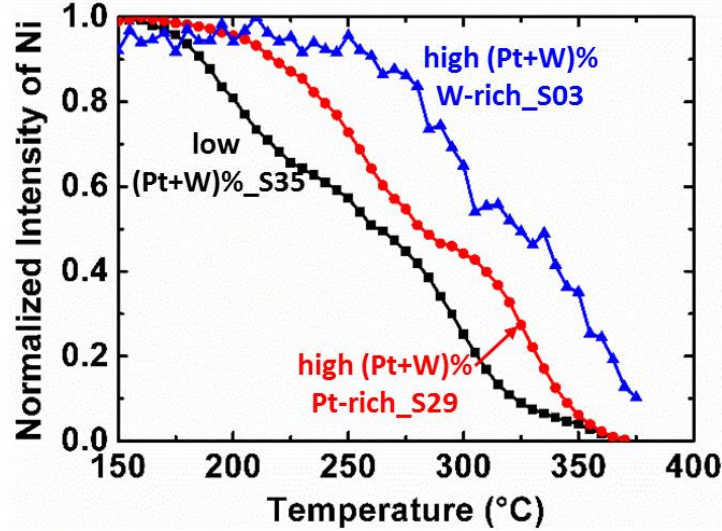


Fig.4. Normalized intensities of the metal peak as a function of temperature for samples with low (Pt+W) contents (S35), high (Pt+W) contents and Pt-rich (S29), and high (Pt+W) contents and W-rich (S03).

In samples with low contents of alloying elements (S35), δ -Ni₂Si forms at 215°C as the first silicide [Fig. 3(a)]. However, no clear information about the first silicide has been provided by *in-situ* XRD measurements for samples with high contents of Pt and W [Fig. 3(b) and 3(c)]. For Pt-rich region (S29), only the metal phase is present until the simultaneous formation of δ -Ni₂Si and NiSi at 280°C. At this reaction stage, around 50% of metal has been consumed. A phase is probably formed by consuming Ni but no relative evidence could be found in XRD. Indeed, the fixed geometry of our XRD equipment may not detect extremely textured or epitaxial phases. It is similar for W-rich sample (S03), where 48% Ni is consumed when the first silicide peak of NiSi is detected at 305°C. This phenomenon of metal consumption without the appearance of other XRD peaks has also been observed in Ni (10 at.% Pt)¹² and in Ni(10 at.%W)⁸. Panciera et. al¹² have shown that the θ -Ni₂Si phase is the first silicide which grows epitaxially on the Si substrate. In our case, we also assume that θ -Ni₂Si forms as the first phase in the samples with high contents alloying

elements but it does not exclude the existence of other unknown phases strongly oriented or epitaxial on Si substrate.

With increasing contents of alloying elements, the first phase is changed from δ -Ni₂Si in S35 to θ -Ni₂Si in S29 and S03. According to El Kousseifi *et al.*¹³, the high solubility of Pt in θ -Ni₂Si should decrease the free energy of θ -Ni₂Si, resulting in a higher driving force and thus a lower nucleation barrier to form θ -Ni₂Si. W may have a similar effect than Pt. Meanwhile, the epitaxial relationship between θ -Ni₂Si and Si leads to a lower energy of θ -Ni₂Si/Si interface and to a further decrease in nucleation barrier. Therefore, with increasing alloy concentration, θ -Ni₂Si could form easily as the first silicide because of the higher driving force of reaction and the lower nucleation barrier.

4.2 Low (Pt+W)% region

For the region of Ni(Pt,W)/Si wafer close to the Ni target, the low contents of (Pt+W) have little impact on the phase sequence but lead to some modifications in the kinetics of phase formation. δ -Ni₂Si and NiSi form sequentially as presented in the schematic diagram [Fig. 5(a)]. Compared to a pure Ni film²², a higher temperature for the total consumption of metal (375°C), a larger temperature range of δ -Ni₂Si from 215°C to 400°C and a late NiSi formation at 375°C have been observed in the *in-situ* XRD measurement of S35 [Fig. 3(a)]. Similar behaviors regarding phase sequence and phase formation kinetics have also been found in Ni with low content of Pt or W (3-5 at. %).^{11,15}

Therefore, for the region with low contents of (Pt+W), the decrease in the Ni diffusion leads to a slower rate of Ni silicides formation, but there is no obvious difference between the effect of individual alloying element (Pt or W) and the combined (Pt+W) effect on the formation sequence

of silicides.

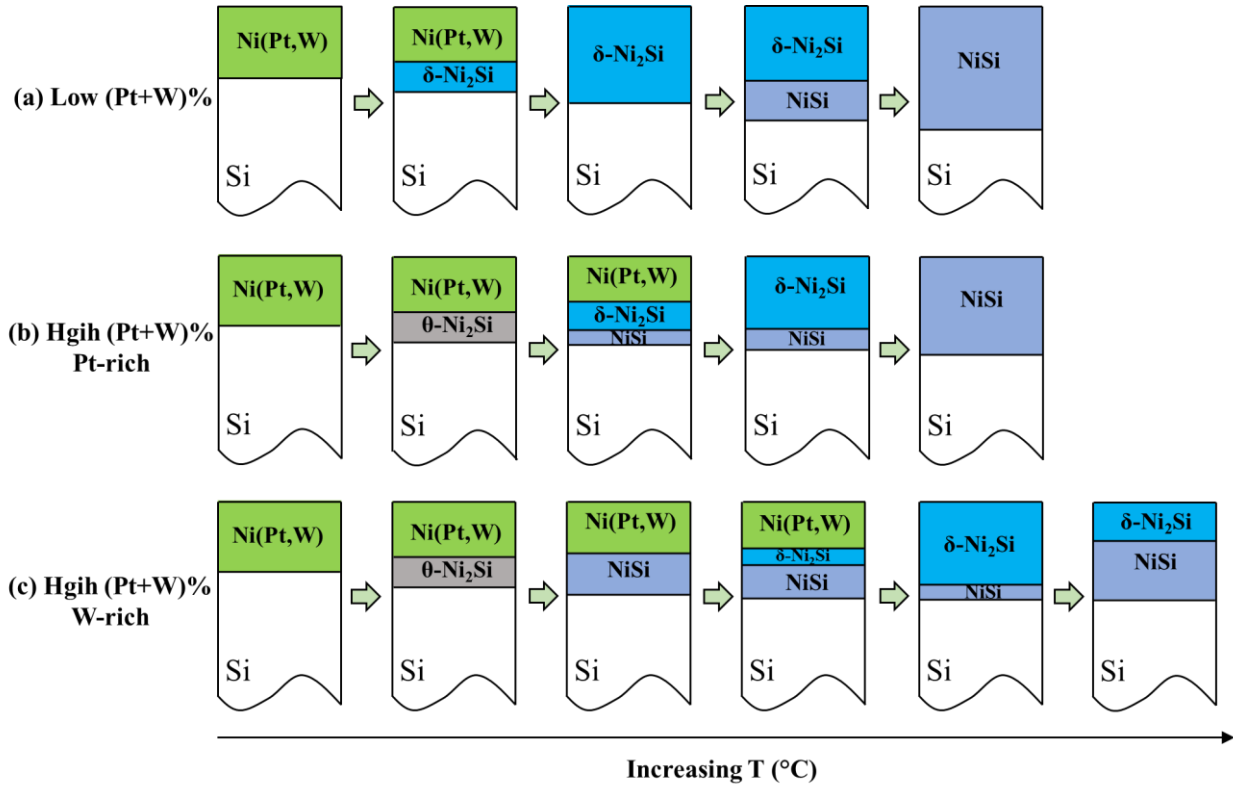


Fig. 5. Schematic diagram for the different phase formation sequence of Ni(Pt,W) film: (a) low (Pt+W)% region, (b) high (Pt+W)% and Pt-rich region, and (c) high (Pt+W)% and W-rich region.

4.3 High (Pt+W)% and Pt-rich region

For the region of Ni(Pt,W)/Si wafer close to the Pt target, a different phase sequence has been observed as compared to the Ni(10 at.% Pt) film.¹² El Kousseifi *et al.*²³ previously reported that the metastable θ -Ni₂Si phase is the only metal rich phase present during the annealing of Ni(10 at.% Pt)/Si and it accounts for the 40°C temperature window without any diffraction peak in the *in-situ* XRD measurement. However, the phase sequence is different in our case as shown in the schematic diagram of important reaction stages [Fig. 5(b)]. θ -Ni₂Si is assumed as the first silicide which consumes 50% of metal when δ -Ni₂Si and NiSi appear simultaneously at 280°C. Before the total

consumption of metal at 370°C, an increase of δ -Ni₂Si peak intensity as well as a stable small peak of NiSi are observed. Afterwards, NiSi grows rapidly by consuming δ -Ni₂Si.

In this high (Pt+W) contents and Pt-rich region, the difference between individual effect of Pt and combined effect of (Pt+W) on phase sequence is relative to the formation of δ -Ni₂Si. The combined presence of Pt and W is more efficient to retard the diffusion of Ni and thus a layer of metal is left when the consumption of θ -Ni₂Si occurs. Therefore, two reactions are competitive as shown in Eq. (3) and (4).



Here, the coefficients of a - d in front of each phase are relative to the chemical composition of θ -Ni_{2-x}Si (i.e., x represents the deviation from stoichiometry). The driving force associated with these reaction are:

$$\Delta G_1 = a \Delta G_{(\delta)} + b \Delta G_{(\text{NiSi})} - \Delta G_{(\theta)} \quad (5)$$

$$\Delta G_2 = \Delta G_{(\delta)} - c \Delta G_{(\text{Ni(Pt,W)})} - d \Delta G_{(\theta)} \quad (6)$$

The decomposition of the metastable θ -Ni₂Si phase [Eq. (3)] requires that the free energy of θ -Ni₂Si (ΔG_{θ}) is higher than that of the mixture of δ -Ni₂Si (ΔG_{δ}) and NiSi (ΔG_{NiSi}). A complex energy balance is associated with this reaction and thus any changes in the interface energy and/or in the free energy of silicides (θ -Ni₂Si, δ -Ni₂Si and NiSi) could easily influence the decomposition of θ -Ni₂Si.²⁴ Panciera *et al.*¹² previously reported that the high solubility of Pt in θ -Ni₂Si could increase the stability of θ -Ni₂Si at low temperature by decreasing its free energy. In our case, the additive W could slow down the diffusion of Ni atoms as well as Pt atoms, even though the content of W is not high in this region. Less Pt atoms could diffuse into the θ -Ni₂Si phase, resulting in a less stable θ -Ni₂Si phase. On the other hand, a slight solubility of W in δ -Ni₂Si and NiSi, which has been

observed in the Ni-Si-W ternary phase diagram,^{25,26} should decrease the free energy of δ -Ni₂Si (ΔG_δ) and NiSi (ΔG_{NiSi}). Therefore, compare to the case of individual alloying element of Pt, the additive W could increase the free energy of θ -Ni₂Si (ΔG_θ) and decrease that of δ -Ni₂Si (ΔG_δ) and NiSi (ΔG_{NiSi}), providing a driving force for the θ -Ni₂Si decomposition.

Moreover, the alloying elements of Pt and W could decrease the free energy of the metal phase ($\Delta G_{Ni(Pt,W)}$), leading to a lower driving force of Eq. (4). Furthermore, the slowing down in Ni diffusion due to the alloying elements should make the occurrence of Eq. (4) even more difficult. Therefore, the decomposition of the θ -Ni₂Si is believed to result in the simultaneous formation of δ -Ni₂Si and NiSi.

4.4 High (Pt+W)% and W-rich region

For the region of Ni(Pt,W)/Si wafer close to the W target, an effect of alloying elements on the texture of NiSi and an interesting reverse phase formation have been observed. Fig. 6 shows the *in-situ* XRD results of three samples of S09, S11 and S13, which are all in this region. With increasing the content of W from S13 to S09, the texture of NiSi changes gradually. As shown in [Fig. 6(d)], the intensities of NiSi(202)/(211) and NiSi(112) peaks decrease while the intensity of NiSi(102)/(111) peak remains stable, which is in agreement with the investigation on Ni(0~7 vol.%W) films by Deduytsche *et al.*⁸ Among all these orientations, the stable orientation of NiSi(102)/(111) is one of the epitaxial components and the decreasing NiSi(202)/(211) texture component corresponds to axiotaxy.⁸ Therefore, an increase in the content of W could improve the stability of NiSi at high temperature by reducing the axiotaxial component of NiSi.

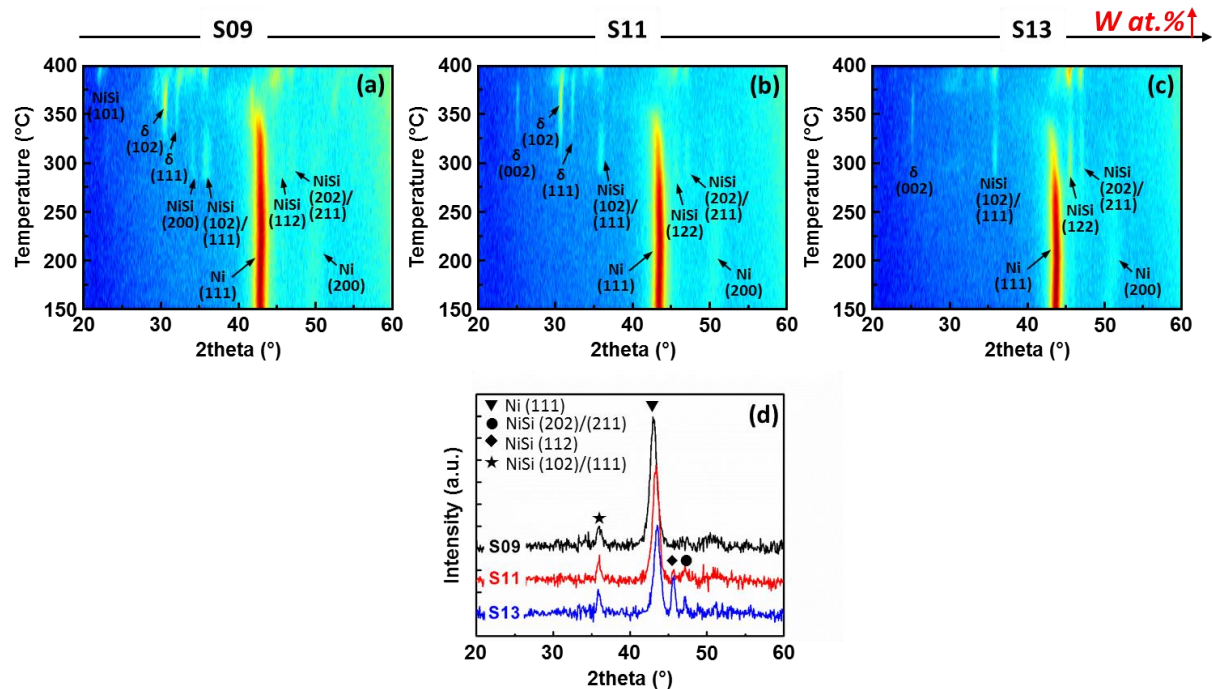


Fig. 6. *In-situ* XRD measurements for high (Pt+W) contents and W-rich samples: (a) S09, (b) S11 and (c) S13; (d) XRD scan at 300°C for S09, S11 and S13.

In this composition region, although the W content varies with the sample position, a similar unexpected phase formation sequence has been found as shown in the schematic diagram [Fig. 5(c)]: NiSi forms at a temperature lower than that of δ -Ni₂Si. When NiSi grows to some extent, δ -Ni₂Si forms and starts to grow by consuming Ni and NiSi. Afterwards, NiSi grows again by consuming δ -Ni₂Si when Ni is completely consumed. In order to clarify this unexpected reverse phase formation, two samples of S12 and S10 were annealed in the *in-situ* XRD chamber using same heat treatment but stopped at 295°C and 345°C, respectively. APT measurements were performed on these two samples: the reconstructed 3D volumes of 20×20×100 nm³ and the corresponding 1D concentration profiles are shown in Fig. 7.

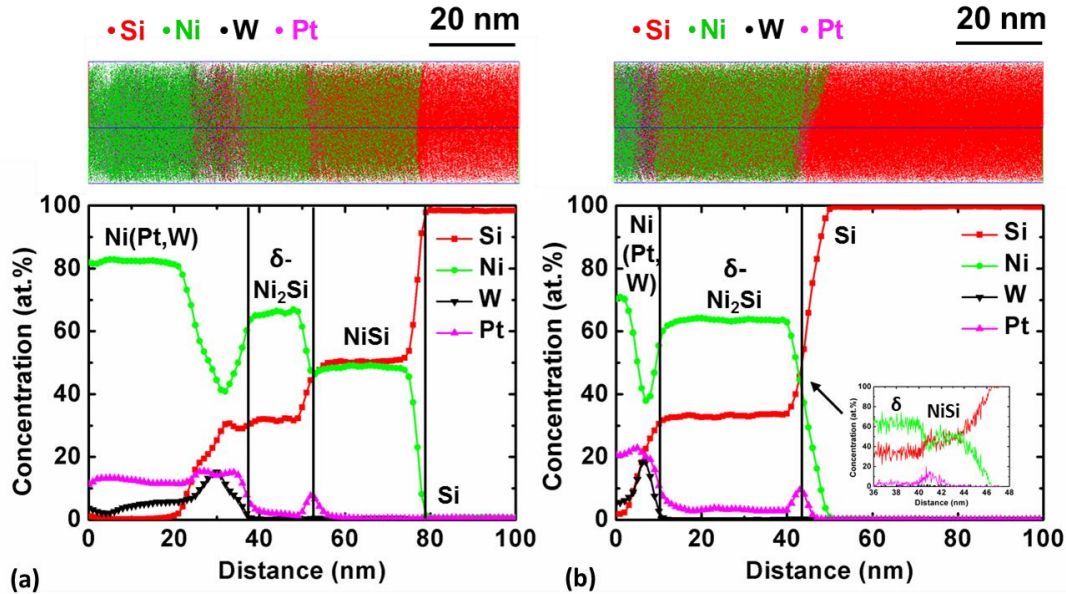


Fig. 7. APT volume and 1D concentration profile of: (a) S12, annealed at 295°C, (b) S10, annealed at 345°C.

Two kinds of silicides could be clearly distinguished between the metal layer and Si substrate for S12 which was annealed up to 295°C [Fig. 7(a)]. The first phase with a 15 nm thickness corresponds to δ -Ni₂Si. The second phase with equal content of Ni and Si could be identified as a 24 nm thick phase of NiSi. Moreover, a mixed layer of around 15 nm enriched with alloying elements is detected between unreacted Ni and δ -Ni₂Si. This region may act as a barrier to slow down the diffusion of Ni. Figure 7(a) also shows the distribution profiles of Pt and W. Pt slightly accumulates in the mixed layer and a gradient of Pt (from 4.8 to 1.4 at.%) appears in δ -Ni₂Si due to the limited solubility of Pt. At this low temperature, Pt could diffuse via the grain boundaries of δ -Ni₂Si and an obvious Pt accumulation is present at the δ -Ni₂Si/NiSi interface. This profile of Pt is relatively similar to what has been observed for Ni with low content of Pt.^{11,27,28} For the distribution of W, there is an obvious accumulation in the same mixed layer where a slight accumulation of Pt is found. In δ -Ni₂Si and NiSi, a low content of W (<0.5 at.%) is observed.

For the other sample (S10), even if the annealing temperature raised up to 345°C, only one thick silicide of δ -Ni₂Si could be clearly recognized in the APT analysis [Fig. 7(b)]. However, a closer look at the 1D concentration computed using fixed sample counting profile [small window in Fig. 7(b)] makes it possible to distinguish a thin layer of NiSi. The alloying elements (Pt and W) are distributed in a similar way as the case of S12 but a slight accumulation of W (~0.3 at.%) was found at the δ -Ni₂Si/NiSi interface. The content of Pt in δ -Ni₂Si is slightly higher, which may be due to the higher annealing temperature.

The APT measurements of samples of S12 (annealed to 295°C) and S10 (annealed to 345°C) verify that δ -Ni₂Si grows at the expense of NiSi, which is consistent with the *in-situ* XRD results for the high (Pt+W) contents with W-rich samples. The accumulated W and Pt in the mixed layer could play a role of barrier to slow down the Ni consumption. The formation of δ -Ni₂Si becomes difficult as lack of the available Ni atoms and then NiSi could form at the Ni/ θ -Ni₂Si interface. With increasing temperature, the diffusion coefficient increases and the function of barrier might be weakened: Ni atoms could diffuse through the mixed layer and δ -Ni₂Si forms by the reaction between NiSi and Ni.

In order to discuss further about the growth of δ -Ni₂Si and NiSi before the total consumption of Ni, a model of simultaneous growth of two phases^{29,30} is introduced. A schematic diagram representing the simultaneous growth of δ -Ni₂Si and NiSi is shown in Fig. 8. The flux of Ni atoms in δ -Ni₂Si (J_1) and in NiSi (J_2) can be expressed as:

$$J_1 = -\frac{2}{\Omega_1} \frac{D_1 \Delta \mu_1}{k_B T} \frac{1}{L_1 + D_1 / K_1} = \frac{2}{\Omega_2} \frac{\alpha_1}{L_1} \quad (7)$$

$$J_2 = -\frac{1}{\Omega_2} \frac{D_2 \Delta \mu_2}{k_B T} \frac{1}{L_2 + D_2 / K_2} = \frac{1}{\Omega_2} \frac{\alpha_2}{L_2} \quad (8)$$

with $\alpha = -\frac{D\Delta\mu}{k_B T}$ and $L' = L + D/L$. The terms α and L' represent the effective diffusivity of Ni

(main diffusing species in δ -Ni₂Si and NiSi) and equivalent thickness of each silicide. D and K are

the diffusion and the interfacial reaction coefficients, and are expressed as $D = D_0 \exp(-\frac{E_D}{k_B T})$,

$K = K_0 \exp(-\frac{E_K}{k_B T})$.³⁰ Ω_1 and Ω_2 are the unit volume of δ -Ni₂Si and NiSi, respectively. There are

three different reactions at the Ni/ δ -Ni₂Si and the δ -Ni₂Si/NiSi interface (Fig. 8). One can easily express the growth of δ -Ni₂Si (L_1) and NiSi (L_2) as:

$$\frac{dL_1}{dt} = \Omega_1(J_1 - J_2) = 2\frac{\alpha_1}{L_1} - \frac{\Omega_1}{\Omega_2} \frac{\alpha_2}{L_2} \quad (9)$$

$$\frac{dL_2}{dt} = \Omega_2(2J_2 - J_1) = 2\frac{\alpha_2}{L_2} - 2\frac{\Omega_2}{\Omega_1} \frac{\alpha_1}{L_1} \quad (10)$$

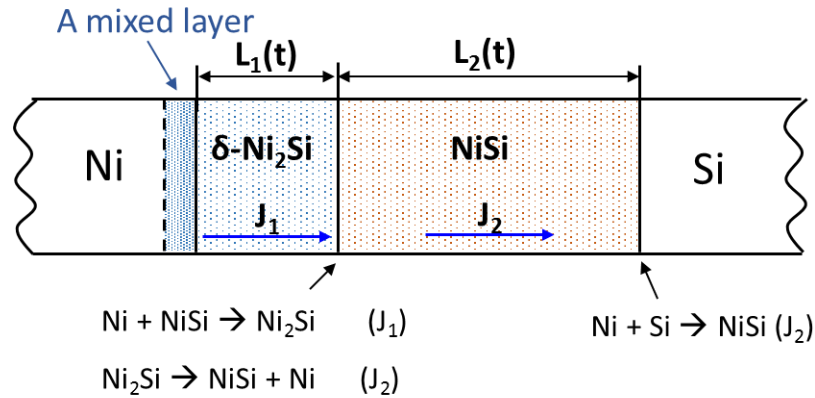


Fig. 8. Schematic diagram of the growth of δ -Ni₂Si and NiSi

At low temperature, the mixed layer enriched with Pt and W could act as a strong barrier, making difficult the diffusion of Ni atoms across this layer and leading to the early formation of NiSi. With increasing temperature, the barrier effect of the mixed layer becomes less strong and δ -Ni₂Si could form between Ni and NiSi. The available Ni film, the smaller thickness of δ -Ni₂Si (L_1), and the

larger thickness of NiSi (L_2) lead to the growth of δ -Ni₂Si ($dL_1/dt > 0$) and the consumption of NiSi ($dL_2/dt < 0$). Therefore, δ -Ni₂Si should grow by consuming NiSi before the total consumption of Ni. When Ni is entirely consumed, the flux J_I equals 0, leading to the regrowth of NiSi by consuming δ -Ni₂Si and Si.

For S09, the intensities of XRD peaks for different silicides are normalized and plotted as a function of time (Fig. 9). The time range starts from the XRD scan at 280°C and ends after the XRD scan at 400°C. As more NiSi orientations appear in the temperature range where NiSi grows by consuming δ -Ni₂Si (the region after 5300s in Fig. 9), different normalization methods were performed on the intensity of NiSi peak. The maximum intensity of NiSi peak is normalized to 1 for the NiSi growth region after 5300s (Fig. 9) and then another factor of 0.6 is used for the NiSi consumption region before 5300s (Fig. 9) in order to guarantee that the sum of normalized intensities for all phases is equal to 1.

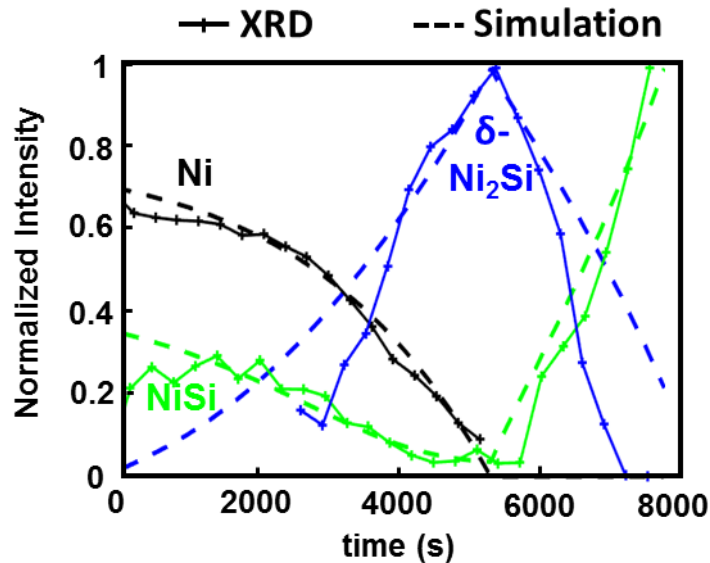


Fig. 9. Comparison between XRD and simulation for the kinetics of silicides growth of S09

Simulation has also been done concerning the reverse phase formation and the following growth behavior of NiSi and δ -Ni₂Si. For S09, the thickness of the as deposited Ni(Pt,W) film is 32nm. 30% Ni has been consumed at 280°C. At this stage, the corresponding thickness of NiSi is around 20nm while the thickness of δ -Ni₂Si is quite small. By assuming an initial state with a 1nm layer of δ -Ni₂Si and a 20nm layer of NiSi, the simulated growth behavior of different phases was shown in Fig. 9 (dash lines). The simulated pre-exponential factors and activation energies of the reaction and the diffusion coefficients are listed in Table 2. For Ni film deposited on single crystalline Si substrate, the activation energy is reported to be ~1.5eV for δ -Ni₂Si growth³¹⁻³³ and (1.55~1.7) eV for NiSi growth.^{32,34} Our simulated activation energies are similar to those found in the literature but the simulated pre-exponential factors are smaller: that might be the effect of alloying elements. Simulation and XRD are in good agreement (Fig. 9), showing that δ -Ni₂Si grows by consuming NiSi and Ni firstly and then NiSi grows again at the expense of δ -Ni₂Si after the total consumption of Ni. This simulation explains the unexpected growth behavior of δ -Ni₂Si and NiSi from the kinetic point of view. The schematics and the model used in the simulation are based on the assumption of one-dimensional growth. However, nucleation at the interface and/or at the triple junction, as well as the lateral growth along interface play an important role in the formation of silicide. This is particularly true for very thin films^{13,23} and may lead to much more complex microstructures. However, for thickness larger than about 10 nm, the nucleation and lateral growth end to a continuous layer which grows then essentially in a one-dimensional manner.

Table 2. Simulated pre-exponential factors and activation energies of the reaction and the diffusion coefficients

	K_0 (cm ² /s)	E_K (eV)	D_0 (cm ² /s)	E_D (eV)
δ-Ni₂Si	0.007	0.8	0.08	1.5
NiSi	0.015	0.9	0.01	1.6

5. Conclusion

Ni(Pt,W) films with thickness and composition gradients have been prepared by co-sputtering of Ni, Pt and W. As-deposited samples were characterized by XRD, XRR, APT and RBS. Simulations of the co-sputtering were carried out for comparison. A good agreement has been found between experimental and simulation results, regarding the thickness and composition of the deposited film. The combined effect of Pt and W on Ni silicides formation has been investigated by *in-situ* XRD measurements and APT. Both Pt and W slow down the Ni consumption rate while the effect of W is more pronounced. Depending on the contents of Pt and W, three regions of the Ni(Pt,W)/Si wafer could be distinguished for the effect of alloying elements on Ni silicides formation. Low contents of (Pt+W) are associated with the region close to the Ni target and have little impact on the formation sequence of silicides: δ -Ni₂Si is the first silicide and NiSi forms when Ni is entirely consumed. For the high (Pt+W) contents and Pt-rich region, except the metal consumption, *in-situ* XRD results do not provide any evidence about the first silicide, which could be θ -Ni₂Si or other unknown phases that are extremely textured or epitaxial on Si. Afterwards, δ -Ni₂Si and NiSi are formed simultaneously which may result from the decomposition of θ -Ni₂Si. For high (Pt+W) contents and W-rich region, the texture of NiSi is changed by reducing NiSi(202)/(211) and NiSi(112), and maintaining the NiSi(102)/(111) peak intensity. An unexpected reverse phase formation is observed: NiSi forms at lower temperature than that of δ -Ni₂Si. The accumulation of alloying elements between unreacted Ni and the first silicide could probably act as a barrier to suppress the diffusion of Ni atoms, leading to an early formation of NiSi. With increasing temperature, the barrier effect of the mixed layer becomes weaker and a larger diffusion coefficient promotes the formation of δ -Ni₂Si at the Ni/NiSi interface. Afterwards, the growth of δ -Ni₂Si and NiSi follow the basic kinetic equations: δ -Ni₂Si grows by consuming

NiSi firstly and after the entire consumption of Ni, NiSi grows again at the expense of δ -Ni₂Si. This behavior has been reproduced by kinetics simulation.

Acknowledgements

Khalid Hoummada and Cherif Benoudia are acknowledged for discussion. The French ministry for education and research is acknowledged for providing the scholarship for the PhD of Ting Luo.

Reference

- ¹ T. Ohguro, S. Nakamura, M. Koike, T. Morimoto, A. Nishiyama, Y. Ushiku, T. Yoshitomi, M. Ono, M. Saito, and H. Iwai, *IEEE Transactions on Electron Devices* **41**, 2305 (1994).
- ² R. Mukai, S. Ozawa, and H. Yagi, *Thin Solid Films* **270**, 567 (1995).
- ³ F. Deng, R. A. Johnson, P. M. Asbeck, S. S. Lau, W. B. Dobbelday, T. Hsiao, and J. Woo, *Journal of Applied Physics* **81**, 8047 (1997).
- ⁴ C. Lavoie, F. M. d'Heurle, C. Detavernier, and C. Cabral, *Microelectronic Engineering* **70**, 144 (2003).
- ⁵ C. Lavoie, C. Detavernier, C. Cabral Jr, F. M. d'Heurle, A. J. Kellock, J. Jordan-Sweet, and J. M. E. Harper, *Microelectronic Engineering* **83**, 2042 (2006).
- ⁶ D. Deduytsche, C. Detavernier, R. L. Van Meirhaeghe, and C. Lavoie, *Journal of Applied Physics* **98**, 033526 (2005).
- ⁷ D. Mangelinck, J. Y. Dai, J. S. Pan, and S. K. Lahiri, *Applied Physics Letters* **75**, 1736 (1999).
- ⁸ D. Deduytsche, C. Detavernier, R. L. Van Meirhaeghe, J. L. Jordan-Sweet, and C. Lavoie, *Journal of Applied Physics* **101**, 044508 (2007).

- ⁹ D. Mangelinck, J. Y. Dai, S. K. Lahiri, C. S. Ho, and T. Osipowicz, *Mater. Res. Soc. Symp. Proc.* **564** (1999).
- ¹⁰ C. Detavernier and C. Lavoie, *Applied Physics Letters* **84**, 3549 (2004).
- ¹¹ J. Demeulemeester, D. Smeets, C. Van Bockstael, C. Detavernier, C. M. Comrie, N. P. Barradas, A. Vieira, and A. Vantomme, *Applied Physics Letters* **93**, 261912 (2008).
- ¹² F. Panciera, D. Mangelinck, K. Hoummada, M. Texier, M. Bertoglio, A. De Luca, M. Gregoire, and M. Juhel, *Scripta Materialia* **78–79**, 9 (2014).
- ¹³ M. El Kousseifi, K. Hoummada, M. Bertoglio, and D. Mangelinck, *Acta Materialia* **106**, 193 (2016).
- ¹⁴ M. Putero, L. Ehouarne, E. Ziegler, and D. Mangelinck, *Scripta Materialia* **63**, 24 (2010).
- ¹⁵ A. Derafa, G. Tellouche, K. Hoummada, A. Bouabellou, and D. Mangelinck, *Microelectronic Engineering* **120**, 150 (2014).
- ¹⁶ X. D. Xiang and I. Takeuchi, *Combinatorial materials synthesis* (Dekker, New York, 2003).
- ¹⁷ L. R. Doolittle, *Nucl. Instrum. Methods Phys. Res. B* **9**, 344 (1985).
- ¹⁸ D. Mangelinck, F. Panciera, K. Hoummada, M. El Kousseifi, C. Perrin, M. Descoins, and A. Portavoce, *Microelectronic Engineering* **120**, 19 (2014).
- ¹⁹ K. Hoummada, C. Perrin-Pellegrino, and D. Mangelinck, *Journal of Applied Physics* **106**, 063511 (2009).
- ²⁰ R. Rother and H. A. Jehn, *Surf. Coat. Technol.* **62**, 635 (1993).
- ²¹ Z. Zhou, W. M. Rainforth, B. Rother, A. P. Ehiasarian, P. Eh. Hovsepian, and W. D. Münz, *Surf. Coat. Technol.* **183**, 275 (2004).
- ²² M. El Kousseifi, K. Hoummada, and D. Mangelinck, *Acta Materialia* **83**, 488 (2015).
- ²³ M. El Kousseifi, K. Hoummada, T. Epicier, and D. Mangelinck, *Acta Materialia* **99**, 1 (2015).

- 24 S. Gaudet, C. Coia, P. Desjardins, and C. Lavoie, *Journal of Applied Physics* **107**, 093515 (2010).
- 25 R. V. Skolozdra, Z. P. Shipka, and E. I. Gladyshevskii, *Inorg. Mater.* **5**, 1250 (1969).
- 26 P. Villars, A. Prince, and H. Okamoto, *Handbook of Ternary Alloy Phase Diagrams*, Vol. 10 (New York, 1995).
- 27 D. Mangelinck, K. Hoummada, A. Portavoce, C. Perrin, R. Daineche, M. Descoins, D. J. Larson, and P. H. Clifton, *Scripta Materialia* **62**, 568 (2010).
- 28 O. Cojocar-Mirédin, D. Mangelinck, K. Hoummada, E. Cadel, D. Blavette, B. Deconihout, and C. Perrin-Pellegrino, *Scripta Materialia* **57**, 373 (2007).
- 29 P. Gas and F. M. d'Heurle, *Applied Surface Science* **73**, 153 (1993).
- 30 T. Barge, P. Gas, and F. M. d'Heurle, *Journal of Materials Research* **10**, 1134 (1995).
- 31 J. O. Olowolafe, M. A. Nicolet, and J. W. Mayer, *Thin Solid Films* **38**, 143 (1976).
- 32 C. D. Lien, M. A. Nicolet, and S. S. Lau, *Thin Solid Films* **143**, 63 (1986).
- 33 K. N. Tu, W. K. Chu, and J. W. Mayer, *Thin Solid Films* **25**, 403 (1975).
- 34 F. d'Heurle, C. S. Petersson, J. E. E. Baglin, S. J. La Placa, and C. Y. Wong, *Journal of Applied Physics* **55**, 4208 (1984).